Pergamon

PII: S0191-8141(96)00087-9

Journal of Structural Geology, Vol. 19, No. 5, pp. 687 to 701, 1997

0191-8141/97 $17.00 + 0.00

The sampling of fault populations in dolerite sills of Central Sweden and implications for resolution of seismic data

C. E. R. LINE*

Bullard Laboratories, University of Cambridge, Madingley Rise, Cambridge CB3 0EZ, U.K.

and

D. B. SNYDER and R. W. HOBBS

BIRPS, Bullard Laboratories, Madingley Rise, Cambridge CB3 0EZ, U.K.

(*Received* 17 *October* 1995; *accepted in revised form* 10 *October* 1996)

Abstract—Geological mapping of faults affecting dolerite sills was carried out along the Baltic coast in central Sweden and scaling relationships for the faults analysed in order to assess the seismic imaging of the sills. The sills are 250–400 m thick and dip at low angle (<20°) to a depth of 10–12 km beneath the Baltic Sea where they are observed as sub-horizontal bright seismic reflections in the BABEL data. Characteristics studied in outcrop included the nature of sill contacts, the horizontal continuity and variations in mineralogy of individual sills, and offsets in the sills by faults. We also compiled, from field observations and detailed geological and tectonic maps, independent data sets on the lengths and displacements of faults. Both fault length and fault displacement populations exhibit power-law scaling over more than 4 orders of magnitude, with exponents that are consistent with a linear relationship between maximum displacement and fault length. The power-law exponent for a one-dimensional fault displacement population is 0.69 ± 0.07, whereas the exponent for a two-dimensional fault length population is 1.66 ± 0.1. These results for the surface were used to predict the perturbation of the seismic reflections caused by deeper faulting in the dolerite sills. Predicted fault displacements would need to be an order of magnitude greater in order to account for the observed segmentation of the seismic reflections. The incoherence in the seismic data is therefore attributed, on the larger scale, to primary structural features of the sills, such as 10-km scale cuspate segments linked by transgressive steps and, on the smaller scale, to the scattering effect of heterogeneities in the overlying crust. © 1997 Elsevier Science Ltd.

INTRODUCTION

The aim of this research is to investigate the effect of scattering of seismic energy on imaging geological structures in a complex upper crust. Seismic scattering, or loss of coherence in the seismic wavefield, is caused by heterogeneities in the crust and by features in the imaged structures. The characteristics of 'known' reflectors at depth in the Earth's crust were inferred from characteristics observed in similar structures at the surface. In this case, the reflectors were dolerite sills that intrude the Palaeoproterozoic crust of the Baltic Shield. The features formed in such bodies as they intrude are largely determined by the magma viscosity and the viscoelastic response of the crust to the intrusion (Pollard *et al.*, 1975). Faulting in the structures is determined by the brittle response of the crust to subsequent tectonic events. The main underlying assumption is that the crust has similar rheology at the depth of the intrusions as it does at the surface: that the crust behaves in a predominantly brittle manner down to a depth of 12 km.

The reflectivity of the sills is characterised by field observations in three main categories: (1) primary features such as continuity, uniformity and relief of the sill contact surfaces and sill thickness variations, (2) mineralogical variations within the dolerite and country rocks, and (3) displacement of the sills by faults. The effect of the former two categories are more fully considered elsewhere. The subject of this paper is the measurement and analysis of faults in the sills: to predict the number of faults per kilometre of reflector along the strike of the seismic profile.

The first part of the paper is concerned with the problems associated with sampling faults over limited areas, and the biasing effects that result in the observed fault populations. In the second part of the paper, synthetic seismograms are generated for reflector models incorporating the statistics of the field data, in order to investigate the resolution of the seismic method in sampling fault populations, and the predicted perturbation to seismic reflections caused by these faults.

GEOLOGICAL SETTING OF THE FIELD AREA

The location of BABEL lines 1, 6 and 7, collected in 1989, are shown in Fig. 1 with the main crustal units of the Baltic Shield. A migrated CMP stack section of the northern part of line 1 (Fig. 2) features a set of sub-horizontal bright crustal reflectors at 3–4 s two-way time with lateral continuity of 50–100 km. These reflectors dip

*Author to whom correspondence should be addressed. E-mail: line@esc.cam.ac.uk.

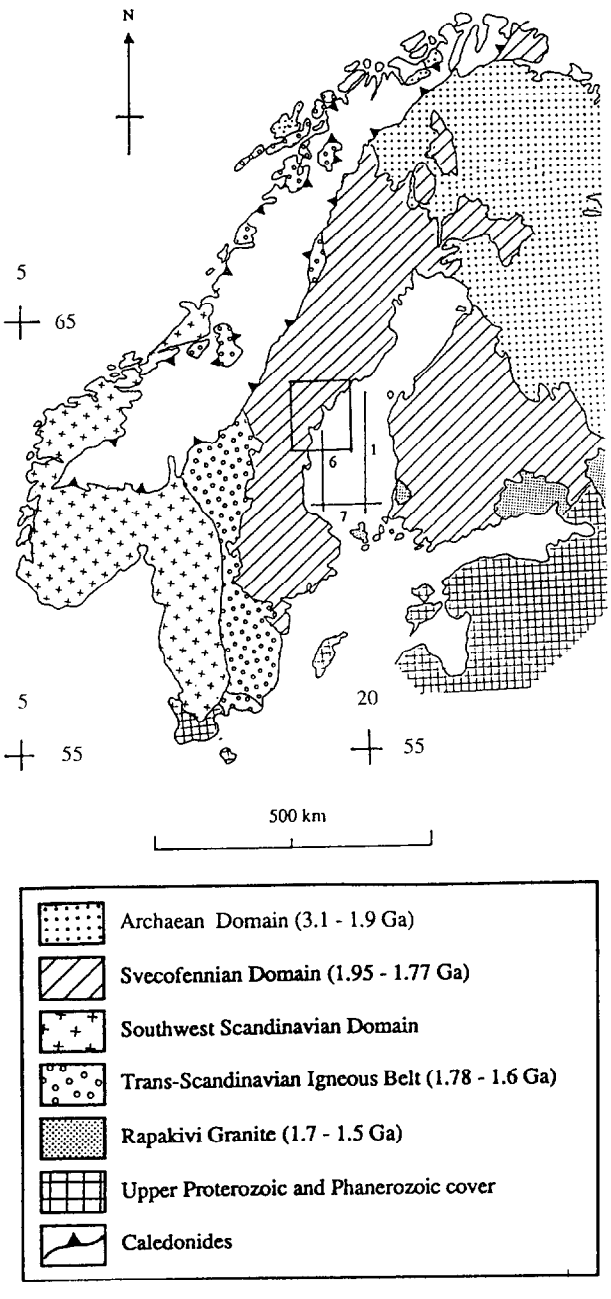

Fig. 1. The Baltic Shield and its major crustal units (adapted from Gaal and Gorbatchev, 1987); also shown are the locations of BABEL lines 1, 6 and 7. Reference latitude and longitude ordinates (N and E, respectively) are shown. The area outlined corresponds to Fig. 3.

gently to the south at the northern end of the section, and are nearly horizontal at the southern end of the section. The reflectors are interpreted as dolerite sills cropping out in Västernorrland county in central Sweden, the mainland adjacent to the northern end of the line (BABEL Working Group, 1993). The sills form part of the Central Scandinavian Dolerite Group (Gorbatchev *et al.*, 1987) and have arcuate exposures ~80 km in diameter (Fig. 3). Field observations and geophysical studies (Lundquist and Samuelsson, 1973; Larson, 1973; Larson and Magnusson, 1979) show that they are 250–400 m thick and dip at 4–20° in directions that vary from east in the south to south in the north.

The bulk of the upper crust in the central Svecofennian province consists of metagreywackes, originally deposited in a basinal (back-arc) facies ~2.0 Ga ago and metamorphosed in the Svecofennian orogeny, 2.0–1.8 Ga ago (Gaal and Gorbatchev, 1987). A number of magmas intruded in the earlier stages of this orogeny (Lundquist, 1973), others in the subsequent anorogenic period, 1.7–1.4 Ga (Welin and Lundquist, 1970). The Jotnian sandstone group was deposited at around 1.3 Ga, and consists of sandstones, intraformational conglomerates and shales (Bergman, 1980) of a shallow marine-shelf, estuarine and/or intertidal origin (Axberg, 1980); the formation dips at 4–10° to the south-east. The Central Scandinavian Dolerite Group intruded the above units during and after the Jotnian period (1.25–1.4 Ga), possibly associated with the early phases of the Sveconorwegian orogeny in the west of Sweden (Welin and Blomquist, 1964). K–Ar radiometric dating of the dolerite at Nordingrå gives an age of around 1.245 ± 0.02 Ga (Welin and Lundquist, 1975). The sills have the character of multiple and layered intrusions; compositional layers and flow-bands 5 cm to 1 m thick are conspicuous in the field, whilst petrographic and palaeomagnetic studies of the sills reveal at least two intrusive units within the sills at Nordingrå and Ulvön (Lundquist and Samuelsson, 1973; Larson, 1973; Larson and Magnusson, 1976; Magnusson, 1983).

No major thermo-tectonic influence has directly affected the area since the Svecofennian orogeny. Palaeomagnetic studies (Larson and Magnusson, 1976) indicate that no major internal block rotations have occurred in the area since Jotnian time. The Sveconorwegian orogeny (1.2–0.9 Ga), Caledonian orogeny (0.6–0.4 Ga) and Tertiary rifting events of the North Sea all occurred to the west, and may have mildly affected the area of the Bothnian Sea by causing re-activation along existing tectonic lines (Axberg, 1980). The same is true of Quaternary crustal loading and unloading caused by the Pleistocene glaciation (Winterhalter, 1972). Most of the faults observed in the field were high-angle normal faults, and all are assumed to have been potentially active during any of these post-Jotnian episodes. In general, dating of post-Jotnian faulting events in the area are poorly constrained. Recent evolution of the Bothnian Bay has been governed by post-glacial crustal rebound, and uplift is still occurring at rates of up to 9 mm per year (Winterhalter *et al.*, 1980).

FIELD MEASUREMENTS

Due to limited inland exposure of the sills, observations were restricted to outcrops along the coast and on the islands of Storön, Ulvön and Trysunda, and at Nordingrå and Skeppsmalen (Fig. 4). Although in some areas the shoreline is either a boulder or gravel beach, or

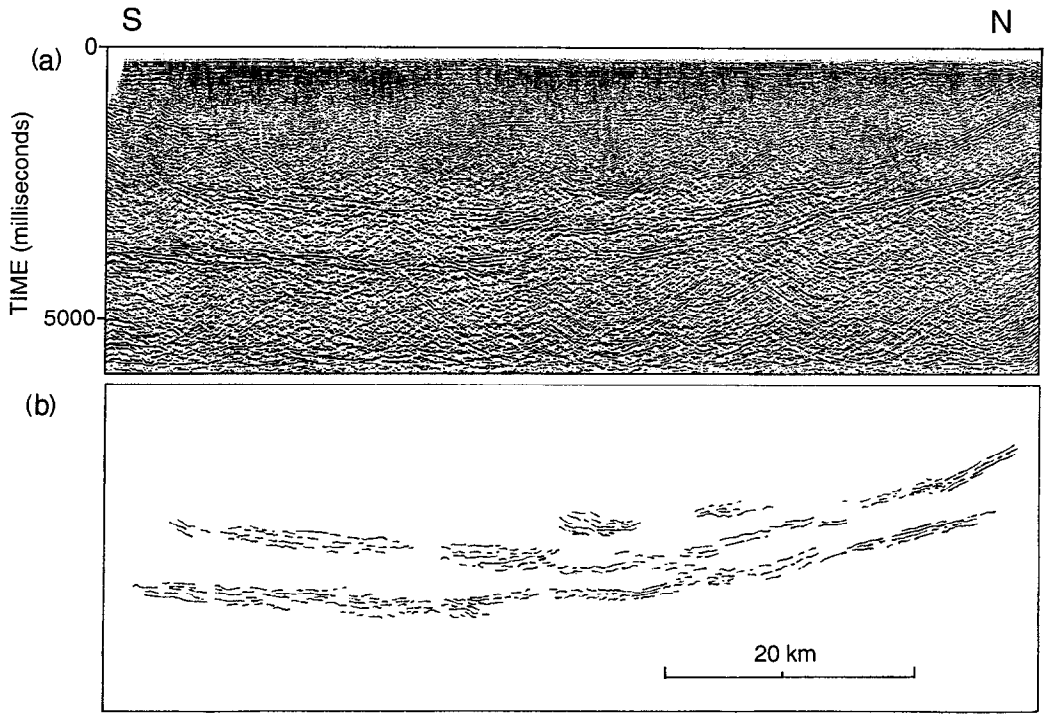

Fig. 2. (a) BABEL line 1 migrated stack, shot points 4205–6182, showing bright sub-horizontal crustal reflections at 3–4 s two-way time (TWT). Main processing steps are: Bandpass filter 5–40 Hz, *f/k* direct wave filter (reject 1.2–2.4 km s^{-1}), *f/k* filter (reject $V \leq 5.0$ km s^{-1}), predictive decon. (48 ms predictive gap), Normal Moveout correction and Stack, Stolt *f/k* migration with a two-dimensional velocity model, AGC (2.0 s window). (b) Line drawing of reflection segments interpreted as dolerite sills.

too steep and precarious to negotiate, in many of the areas studied the rocks are polished smooth and flat by glacial action and exposed in pavements 10–100 m wide. In the following sections distinction is made between primary structural features—characteristics of the crack propagation processes that occurred during formation of the sill—and secondary features such as subsequent faulting in the sill.

Primary structural features

The general form of the sills has been described as *lopolithic*, or dish-shaped, by other workers (Lundquist and Samuelsson, 1973). Between Örnsköldsvik and Husum a sill is intruded in en échelon sections of lengths between 5 and 30 km (Fig. 3). Insufficient information exists to determine whether the exposures at Skeppsmalen (Skaggsudde), Trysunda, Ulvön and Nordingrå (Fig. 4) are connected either under water or at depth in the crust.

The contact between the dolerite and the Jotnian sandstone is generally sub-parallel to bedding and has little relief. Steps of 0.5–1 m in the level of the lower contact were observed at Storön with a spacing of 10–20 m. Secondary sills up to 2 m thick often occur a few metres above or below the main (i.e. at Storön, Skeppsmalen, and Trysunda). The contact between the dolerite and other rock units such as the Nordingrå granite at Ulvön appears, at least on the large scale, to be more variable, with a relief of amplitude up to 50 m and wavelength of around 2 km. A large number of dikes, of composition varying from basaltic to felsic, were observed in the field; dike thicknesses reach 7 m, but are mostly less than 1 m. Thus the number of feeder dikes observed in the area that are likely to disrupt the continuity of the seismic reflections is very small.

Large-scale sill geometry thus seems to be characterised by a primary segmentation in the sill of length-scales between 5 and 30 km, and within these sections a smoothly-varying relief of up to 50 m with a wavelength of around 2 km.

Velocity determination

Determinations of mineralogy of the dolerite were carried out by the principal author from point-counts of thin sections taken from field samples, and *in situ* measurements of seismic velocity were made on the dolerite and the country rocks using ultra-sonic testing equipment. Although prominent petrological and mineralogical layering is evident in vertical profiles of the sills (Lundquist and Samuelsson, 1973; Larson, 1973; Larson and Magnusson, 1976), mineralogy determinations and velocity measurements show that the dolerite is very uniform in composition along the plane of intrusion. Thus, in terms of lateral variability in sill reflectivity, compositional variations are considered a second order

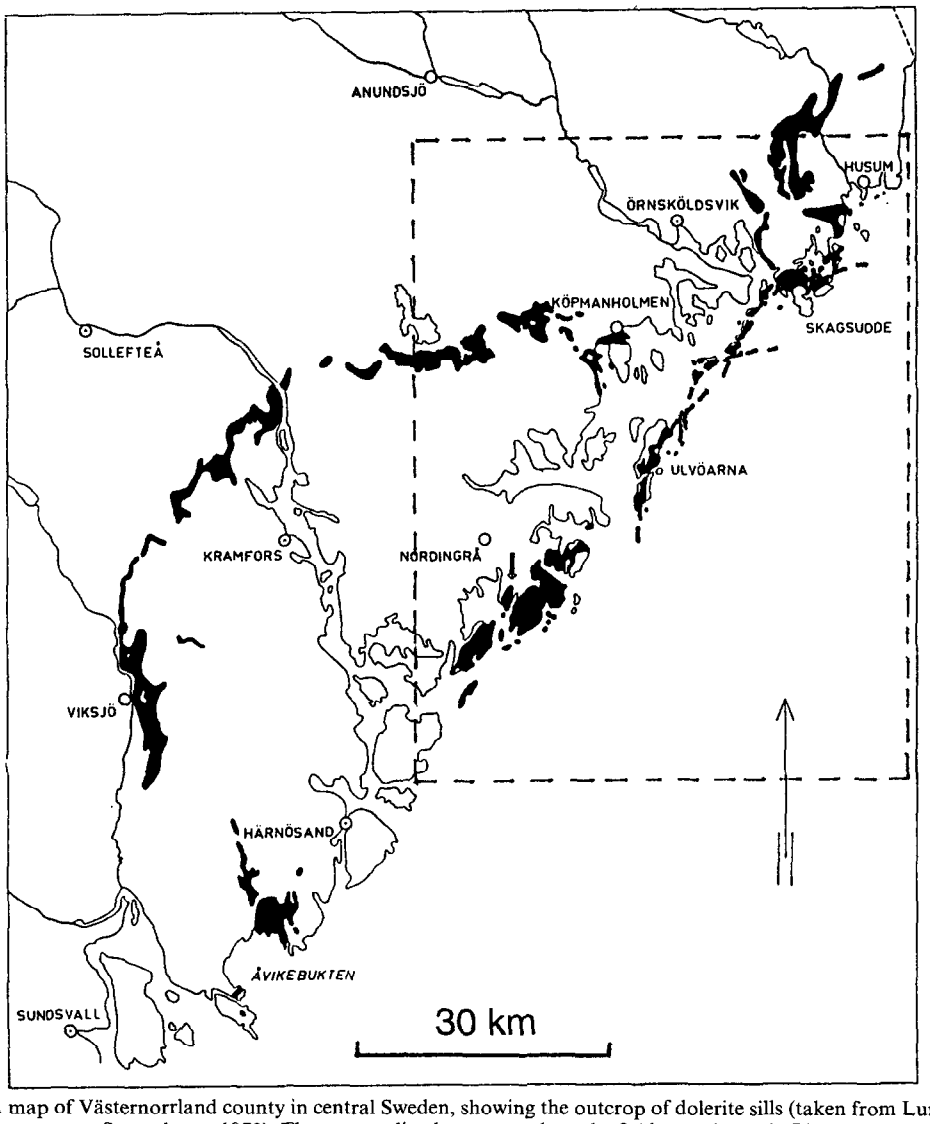

Fig. 3. A map of Västernorrland county in central Sweden, showing the outcrop of dolerite sills (taken from Lundquist and Samuelsson, 1973). The area outlined corresponds to the field area shown in Fig. 4.

effect compared to structural features developed in the sill surfaces.

Faults

Due to the limited nature of the exposure, and the fact that most of the rocks in the field area are igneous, reliable measurements of both displacement and length over several orders of magnitude were not possible. In a few areas it was possible to collect independent data sets of fault lengths and fault displacements.

The best areal exposure of bedrock was found at Rotsidan on the Nordingrå peninsula (Fig. 4), where a data set of 134 faults with lengths of 8–200 m was collected on a coastal dolerite pavement 4 km long and 50–150 m wide. Many of the faults terminate at intersections with other faults. In such cases, the subsidiary branch was considered as a separate fault. Faults and joints initiated at depth were identified by the presence of minerals such as calcite, epidote, chlorite and sericite on the fracture surfaces. Offsets could not be reliably measured due to a lack of piercing points at this exposure. In the absence of piercing points faults were distinguished from joints by the presence of slickenfibers and slickenlines on the fracture surfaces, and in the case of larger faults, by cataclasite.

At Trysunda and Storön (Fig. 4) 100 fault throws, between 1 cm and 7 m, were measured in Jotnian sandstone immediately beneath the lower dolerite contact, continuously exposed over a total of 2.8 km of coastline. Faults mapped included all observed fractures with a visible throw of 0.5 cm or more; fractures with a throw less than this were discarded as joints. Along the narrow exposures on these islands, faults and joints were often observed through the entire exposed section and were sub-vertical.

Large-scale fault displacements in the Ulvö sill were obtained from field geological maps (e.g. Fig. 4). A throw

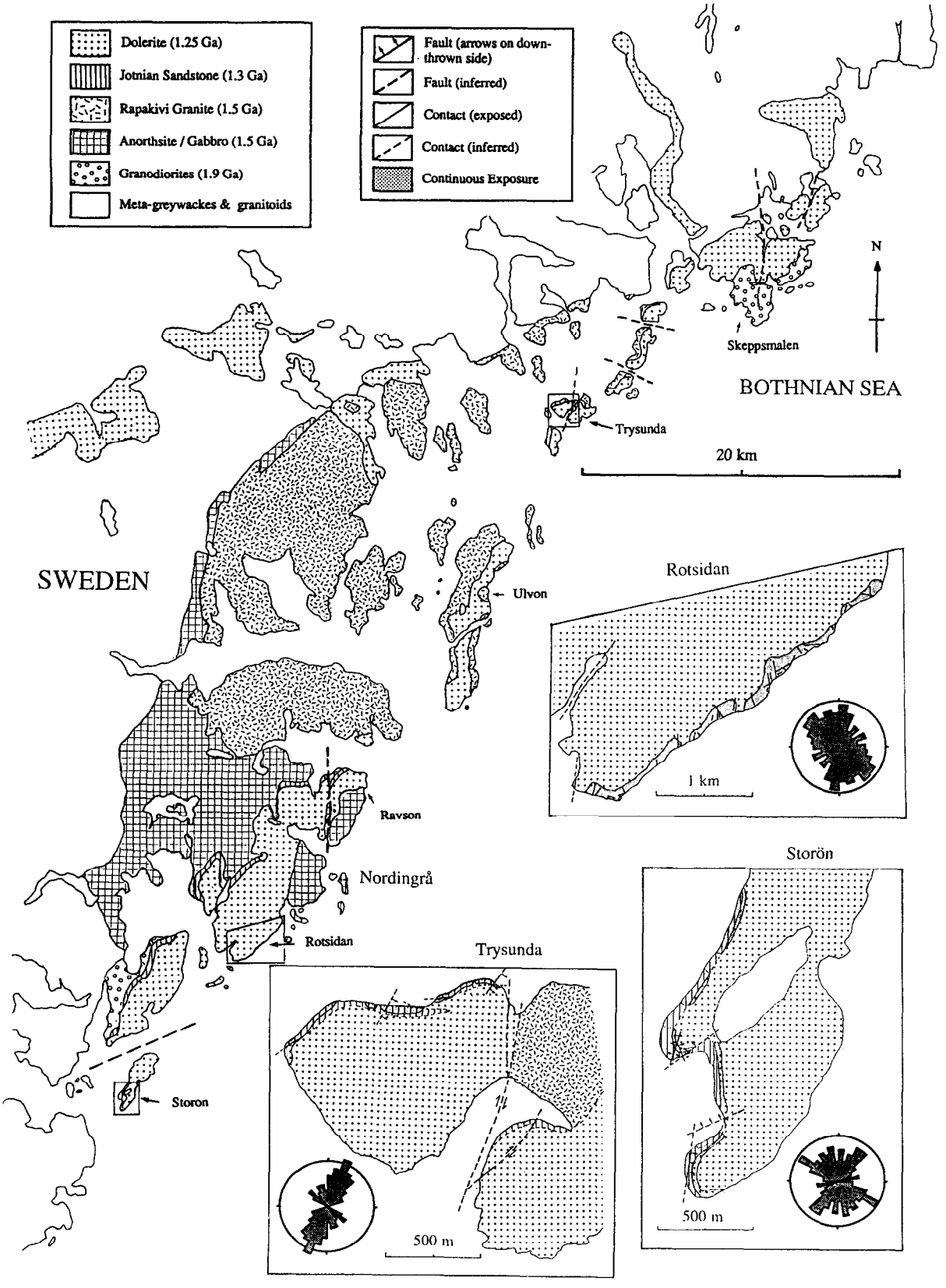

Fig. 4. A geological map of the field area obtained from field mapping, and based on published maps (SGU SER. Ba NR 31), showing the Ulvö dolerite sill and the main rock groups into which it intrudes. Inset are locations (Rotsidan, Trysunda and Storön) where faults were measured, with the positions of the major faults. Rose diagrams show the orientation distributions of the observed fault populations.

was calculated from the horizontal offset in the sill outcrop and the local dip of the sill; 8 faults with throws of at least 50 m were found along the 60 km of continuous outcrop. Large-scale fault lengths were measured on fault trace maps of the Bothnian Sea (Fig. 5) derived from bathymetric data (where the faults are visible as fault line scarps) and from shallow seismic reflection and refraction profiles.

The Bothnian Sea depression is occupied by up to 100 m of Upper Proterozoic and Lower Paleozoic (e.g. Cambrian and Ordovician carbonate) sedimentary rocks overlying the Precambrian bedrock, covered by Quaternary sediments, 10s of metres thick (Winterhalter, 1972; Axberg, 1980) consisting of glacial drift, tills, clays and glaciofluvial accumulations, plus small amounts of post-glacial sediments. These sediments pre-date the majority of the faults in the Bothnian Bay, and decrease the resolution of the fault map in Fig. 5. Orientation distributions for the faults measured in the field area and from the fault trace map of the Bothnian Sea are shown in Figs 4 & 5. Faults at Rotsidan (Fig. 4) and in the Bothnian Bay (Fig. 5) show predominant trends

Fig. 5. Fault trace map of the Bothnian Sea, derived from bathymetric maps and shallow seismic reflection and refraction profiles (taken from Axberg, 1980). The rose diagram shows the distribution of fault strikes.

between N30°W and N30°E. Faults at Trysunda are predominantly sub-parallel with the large bounding fault there, and those at Storön show dominant NW and NE trends.

THEORETICAL AND OBSERVED FAULT RELATIONSHIPS

Worldwide data sets of fault length L and fault displacement D have been shown to obey a power-law (Kakimi, 1980; Walsh *et al.*, 1991; Jackson and Sanderson, 1992; Marrett and Allmendinger, 1992; Scholz *et al.*, 1993):

$$N(D) = B_D D^{-c_D} \quad (1)$$

$$N(L) = B_L L^{-c_L}. \quad (2)$$

N signifies cumulative number of faults (all faults with displacements or lengths greater than or equal to D or L, respectively) and B_D, B_L, c_D and c_L are constants. In order for the power-law to be justified, the exponents c_D and c_L are estimated from the slope of log–log plots over several orders of magnitude. Exponent values derived by the different authors have varied considerably according to the lithology, the tectonic environment, and sampling dimension.

Providing $c_D = c_L = c$, such distributions imply a linear relation between maximum displacement on a fault D_o and its size, or length at outcrop L (Marrett and Allmendinger, 1991), a relationship that has also been observed in fault data sets (Scholz and Cowie, 1990; Scholz *et al.*, 1993):

$$D_o = \gamma L. \quad (3)$$

This relationship is predicted by Dugdale–Barenblatt elastic–plastic fracture mechanics assuming a uniform lithology and depth of burial and constant remote tectonic stress (Cowie and Scholz, 1992). It implies that fault growth is a self-similar (fractal), or scale-invariant, process. At all scales between specified fractal limits, any portion of a self-similar process is a scaled down version of the whole (Gillespie *et al.*, 1993).

SAMPLING CONSIDERATIONS

The nature of the fault sampling method used is of great importance in determining fault populations and strain estimates (e.g. Marrett and Allmendinger, 1991). Sampling of faults in two dimensions is the measurement of faults lying within a large area, where the dimensions of the sampling area are much larger than the maximum fault length of interest. Sampling of faults in one dimension is the measurement of faults intersecting a transect. In both cases fault sampling is biased relative to both fault length and orientation. Distributions observed in a data set will thus be different according to whether sampling one or two dimensions. The fault lengths measured at Rotsidan and from tectonic maps of the Bothnian Sea are sampled in two dimensions, whereas the fault displacements observed along the shorelines of Trysunda and Storön are sampled in one dimension. This research attempts to combine the two-dimensional distribution of fault length and one-dimensional distribution of fault displacement.

Two effects that cause deviation from the expected power-law distribution in a one-dimension fault population are truncation and censoring (Jackson and Sanderson, 1992; Pickering *et al.*, 1994). A sampled population will have a limit of resolution imposed by factors such as the thickness of the marker beds used at outcrop, or the seismic wavelength for faults interpreted from seismic data. Under-sampling of faults close to the limit of resolution leads to truncation, or a decrease in the slope of the cumulative frequency plot for the smaller faults in the population. Conversely, the largest faults in the population will be under-sampled if they have low probability of occurring within the sampling area. Sections of outcrop are often bounded by large faults which cannot be observed themselves. This is known as censoring, and increases the slope of the cumulative frequency plot for the larger faults in the population.

Similar effects arise in two-dimensional sampling of fault lengths. As displacement resolution decreases (for example due to sediments masking the scarps of faults interpreted from bathymetric data), the length of each fault will decrease. This leads to a decrease in the slope of the observed fault length population (Watterson *et al.*, 1995). Edge effects occur for faults that extend out of the sampling area, where measured fault lengths are less than actual fault lengths. This leads to a misrepresentation of the largest faults within the limits of the sampled population and a resulting decrease in the measured exponent of the power-law distribution (Laslett, 1982).

THEORETICAL DERIVATIONS

In the following section F is used to denote cumulative frequency, or numbers per km^2 (two-dimensional sampling) or per km (one-dimensional sampling). This is to enable the comparison and joint analysis of fault data collected from different sampling areas or lengths of transect. The straight line fit on a log–log plot of $F(L)$ (Fig. 6, to be derived), shows that fault lengths observed in the area of the Bothnian Bay obey a power-law. The two-dimensional cumulative frequency of fault lengths within a large area is given by the 'regional distribution':

$$F(L) = BL^{-c_2}. \quad (4)$$

In the following section expressions are derived for the distribution of fault displacements sampled along a

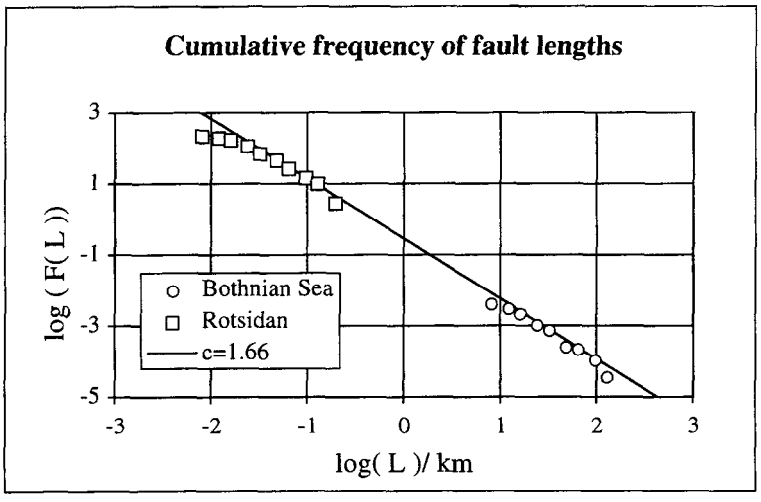

Fig. 6. Cumulative frequency of fault length (L) from field observations at Rotsidan, Nordingrå (squares) and from the fault line map, Fig. 5 (circles). The data are corrected for edge effects (Rotsidan faults) and displacement resolution (Bothnian Sea faults). Error bars, calculated from uncertainties in the sampling area, are approximately equal to the size of the symbols.

transect (in one dimension) or within a sampling swathe (in one and a half dimension), assuming:

(1) A linear displacement–length relationship (Eq. (3)).

(2) N is described by two independent functions; a strike distribution function $\Phi(\phi)$, normalised as follows:

$$\int_0^{\pi} \Phi(\phi)\mathrm{d}\phi = 1 \qquad (5)$$

and a fault density function $\rho(L)$ where $\rho(L)\mathrm{d}L$ is the number of faults of length $L \pm \mathrm{d}L/2$ (km) per km^2: Since

$$F(L) = \int_L^{\infty} \rho(L')\mathrm{d}L',$$

differentiating yields

$$\rho(L)\mathrm{d}L = \frac{\mathrm{d}F}{\mathrm{d}L} = c_2 B\, L^{-(c_2+1)}\mathrm{d}L. \qquad (6)$$

The displacement profile for the faults (i.e. variation in displacement along the length of each fault) also needs to be estimated. Whilst in reality displacement profiles will be fairly irregular and vary between faults, two specific cases are considered (Fig. 7). The first is one of approximately constant displacement along the length of the fault except near the tip-line, where it decreases to zero, described as an M-type profile in Muraoka and Kamata (1983). The second is one where displacement increases linearly from zero at the tip-line to a maximum at the fault midpoint; this approximates the 'cumulative slip profile' of Walsh and Watterson (1987) and is referred to by Muraoka and Kamata (1983) as C-type (cone-shaped). These two models provide bounds on the expected average displacement profile for the fault population, which is assumed to be some intermediate case, e.g. the ideal elastic (I-type) profile of Pollard and Segall (1987) or E-type (elevated) profile (Peacock, 1991; Peacock and Sanderson, 1991).

MODEL 1: NEAR-CONSTANT DISPLACEMENT OR M-TYPE PROFILE

The relationship between fault length distributions and fault displacement distributions is first established for the M-type profile, which simplistically assumes that the displacement measured on a fault is always close to the maximum displacement. In this case the number of faults

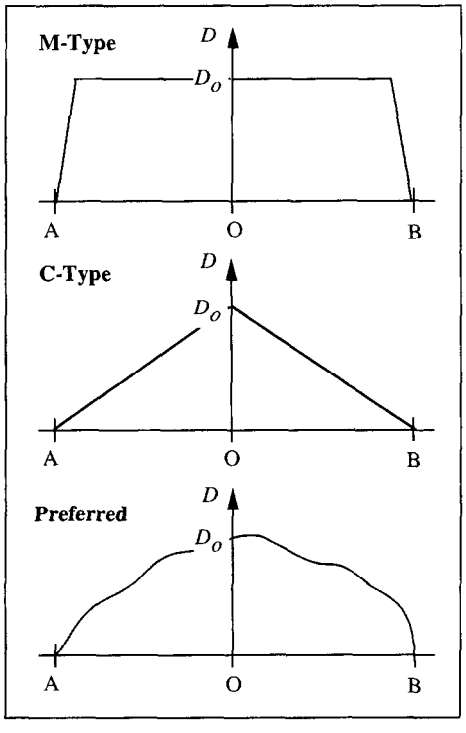

Fig. 7. An illustration of an M-type, C-type and a preferred 'real-world' fault displacement profile. The actual fault displacement profiles occurring in the field area, whilst expected to be variable and irregular, are assumed to be intermediate cases of the M-type and C-type profiles.

of length $(L \pm dL/2)$ and strike $(\phi \pm d\phi/2)$, or the 'discrete frequency' F', observed per km along a swathe of strike θ and width W is given by:

$$F'(L, \phi) = (W + L \sin(|\phi - \theta|))\, \rho(L)\, dL\, \Phi(\phi)\, d\phi.$$

From Eq. (6)

$$F'(L, \phi) = (W + L \sin(|\phi - \theta|))\, c_2\, B\, \Phi(\phi) d\phi\, L^{-(c_2+1)}\, dL.$$

Integrating over the interval $\pi \geq \phi > 0$ and for all $L' \geq L$ yields:

$$F(L) = c_2\, WB \int_L^\infty L^{-(c_2+1)}\, dL \int_0^\pi \Phi(\phi)\, d\phi +$$

$$c_2\, B \int_L^\infty L^{-c_2} dL \int_0^\pi \Phi(\phi) \sin(|\phi - \theta|)\, d\phi. \quad (7)$$

From Eq. (5)

$$F(L) = WBL^{-c_2} + \frac{c_2 BG(\theta)}{(c_2 - 1)} L^{-c_2+1} \quad (8)$$

where

$$G(\theta) = \int_0^\pi \Phi(\phi) \sin(|\phi - \theta|)\, d\phi. \quad (9)$$

From Eq. (3)

$$F(D) = \gamma^{c_2} WBD^{-c_2} + \frac{\gamma^{c_2-1} c_2 BG(\theta)}{(c_2 - 1)} D^{-c_2+1}. \quad (10)$$

Equation (10) gives the cumulative distribution of faults observed per km along a transect striking θ, where the width of the sampling swathe is W. The first term is the contribution from two-dimensional sampling of the fault population. This term dominates when the swathe width is much greater than the minimum fault length of interest. The second term is the contribution from one-dimensional sampling. It dominates when the smallest faults of interest completely traverse the sampling area.

The term $G(\theta)$ given by Eq. (9) is the orientation factor. It represents the dependence of the one-dimensional fault sampling on profile strike; for a fault population wholly oriented in one strike direction this will vary between 1.0 and 0.0, at strikes perpendicular and parallel to the fault orientation respectively. For faults with no preferred orientation ($\Phi = 1/\pi$), $G(\theta)$ will be constant at $(2/\pi)$.

MODEL 2: CONE-SHAPED OR *C*-TYPE DISPLACEMENT PROFILE

The displacement measured on a fault where it intersects the sampling transect will generally be less than its maximum displacement, D_o. This is illustrated in Fig. 8 for a *C*-type displacement profile. For a fault AB, strike ϕ, with midpoint O a distance H from the transect, strike θ, the displacement measured on the transect (at X) is:

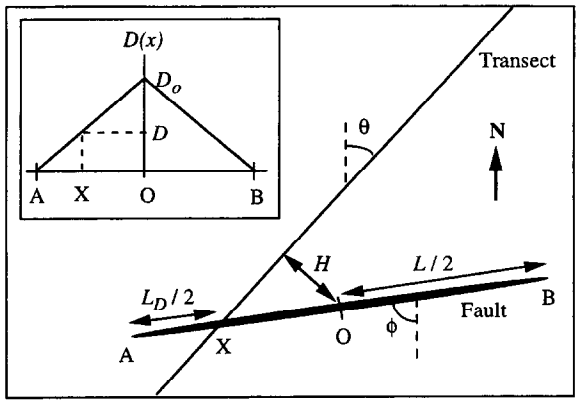

Fig. 8. Sampling faults with a *C*-type displacement profile (shown inset) along a transect. The actual displacement measured $D \leq D_o$, the maximum displacement. H is the distance of the midpoint O from the transect, X is the intersection of the fault with the transect, and the length of the fault AB is a distance L. θ and ϕ are strikes of the transect and fault, respectively. $D_o/L = D/L_D = \gamma$.

$$D = \gamma L_D \quad (11)$$

where

$$L_D = L - \frac{2H}{\sin(|\phi - \theta|)} \quad (12)$$

and $H < (L/2)\sin(|\phi - \theta|)$. From Eq. (12) the discrete frequency of faults of length $(L_D \pm dL_D/2)$ and strike $(\phi \pm d\phi/2)$ intersecting the sampling transect is given by

$$F'(L, \phi) =$$

$$2 \int_{H=0}^\infty \rho\left(L_D + \frac{2H}{\sin(|\phi - \theta|)}\right) dL_D\, dH\, \Phi(\phi)\, d\phi.$$

From Eq. (6) $F'(L, \phi) = B \sin(|\phi - \theta|)\, \Phi(\phi)\, L_D^{-c_2}$. (13)

Integrating over the interval $\pi \geq \phi > 0$ and for all $L' \geq L$ yields

$$F(L_D) = \frac{BG(\theta)}{(c_2 - 1)} L_D^{-c_2+1}. \quad (14)$$

From Eq. (11)

$$F(D) = \frac{\gamma^{c_2-1} BG(\theta)}{(c_2 - 1)} D^{-c_2+1}. \quad (15)$$

Equation (15) corresponds to the one-dimensional term of Eq. (10). Defining the observed (one-dimensional) fault displacement distribution by a power-law function:

$$F_{1D}(D) \equiv AD^{-c_1} \quad (16)$$

and equating with the one-dimensional term for the case of an *M*-type profile (Eq. (10)) yields

$$AD^{-c_1} \equiv \frac{\gamma^{c_2-1} c_2 BG(\theta)}{(c_2 - 1)} D^{-c_2+1} \quad (17)$$

whereas for a C-type profile (Eq. (15))

$$AD^{-c_1} \equiv \frac{\gamma^{c_2-1} BG(\theta)}{(c_2-1)} D^{-c_2+1}. \quad (18)$$

The difference of the factor c_2 in Eqs (17) and (18) arises from the different assumptions made regarding the displacement profile of the faults. Both imply $c_1 = c_2 - 1$ (i.e. the power-law coefficient of the one-dimensionally sampled fault displacements is 1 less than that of the regional cumulative distribution; Marrett and Allmendinger, 1991). The relationship between the constants A, B, $G(\theta)$ and γ is also derived.

RESULTS

Fault lengths

Cumulative distributions of fault lengths from Rotsidan and from the Bothnian Sea were corrected for edge effects and displacements resolution effects, respectively. Edge effect corrections were estimated following Laslett (1982), assuming (as an approximation) a sampling area that is 4 km long and 100 m wide, and an isotropic orientation distribution. Displacement resolution corrections were estimated assuming that all measured fault lengths are truncated by 1 km, corresponding to a vertical resolution limit of 50 m (for a C-type profile and $\gamma = 0.05$, derived below). This is the approximate thickness of the Quaternary sediments in the Bothnian Sea (Winterhalter, 1972; Axberg, 1980).

Although there is a lack of data in the mid-range, the whole data set fits a power-law (Fig. 6); the power-law exponent was estimated by linear regression. Before the above corrections the exponent was 1.73; after corrections the exponent is 1.66. Each data set is subject to a systemmatic vertical error due to uncertainty in the sampling areas, approximately equal to the size of the symbols.

Fault displacements

Cumulative distributions of fault displacements observed at Trysunda, Storön and from geological maps were corrected for censoring, following Pickering *et al.* (1994), where a constant value N_c, corresponding to the number of large faults 'missed' by the sampling, is added to each data point. If N_s is the number of faults sampled, between minimum and maximum displacements of $D_{\min}$ and $D_{\max}$, respectively, and N_T is the total number of faults of displacement greater than or equal to $D_{\min}$, then N_c is given (from Eq. (4)) by

$$\log N_c = \log N_T - c_1 (\log D_{\max} - \log D_{\min})$$

or

$$\log N_c \approx \log N_s - c_1 (\log D_{\max} - \log D_{\min})$$

provided $N_s \gg N_c$.

N_c, calculated for the small-scale data ($N_s = 100$), is 0.8 faults over the outcrop length (2.8 km). For the large-scale data ($N_s = 8$) N_c is estimated as 1.9.

The whole data set shows a fit to a power-law (Fig. 9). Before censoring corrections, the power-law exponent was 0.74; after the corrections the exponent is estimated as 0.69.

The error bounds on the power-law coefficients were estimated using the empirical expressions developed by Pickering *et al.* (1994) (the numbers given are empirical values):

$$68\% \text{ Interval} \approx \pm 0.075 \sqrt{\frac{200}{N_S}} c_1 \quad \text{and}$$

$$95\% \text{ Interval} \approx \pm 0.15 \sqrt{\frac{200}{N_S}} c_1.$$

The derived power-law coefficient for the one-dimensional fault displacement data is 0.69 ± 0.07 to 68% uncertainty, and 0.69 ± 0.14 to 95% uncertainty, compared to 1.66 ± 0.10 at 68% and 1.66 ± 0.20 at 95% for the two-dimensional fault length data.

The cumulative fault spacing distribution is obtained from the distance along continuous exposure between adjacent faults, and is shown for the faults observed at Storön and Trysunda (Fig. 10). Gillespie *et al.* (1993) generated similar plots for one-dimensional synthetic fault populations with spatial distributions that were, in order of increasing clustering, (i) uniform, (ii) random, (iii) generated by a Komolgorov fragmentation process and (iv) fractal. By comparison of these with Fig. 10, we conclude that the one-dimensional spatial distribution of faults at Storön and Trysunda is predominantly random with weak clustering, rather than power-law (fractal). The distribution of fault spacings for the larger faults only (e.g. $D > 10$ cm) is essentially unchanged.

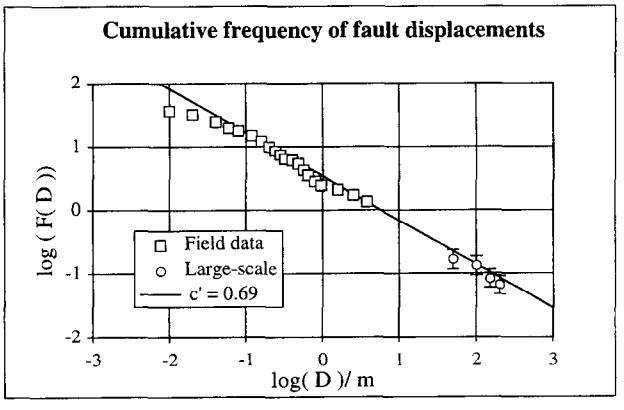

Fig. 9. Cumulative frequency of fault displacements (D) from field observations at Trysunda and Storön (squares) and from geological maps (circles). The data are corrected for censoring (following Pickering *et al.*, 1994). Error bars are calculated using Poisson statistics, where a count of N_s from a random population is subject to a % counting error of $1/\sqrt{N_s}$. For the field data, such errors are less than or equal to the size of the symbols.

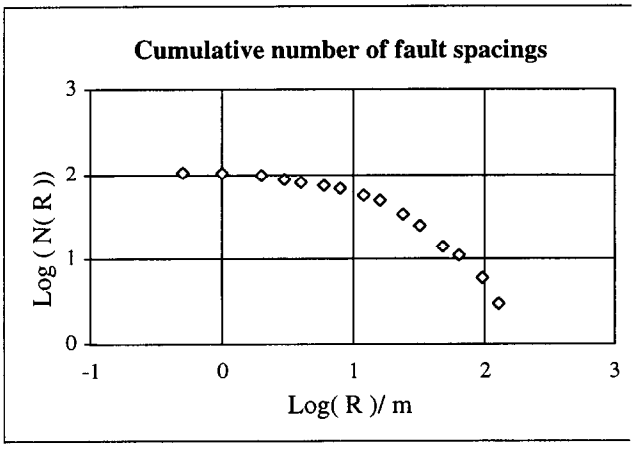

Fig. 10. Cumulative number of fault spacings (R) observed at Trysunda and Storön. The distribution is approximately negative-exponential and consistent with a one-dimensional fault population of random, or Poisson spatial distribution (Gillespie *et al.*, 1993).

CALCULATIONS

Assuming that the fault length and fault displacement distributions observed are consistent (i.e. all faults are sampled from the same power-law distribution), either the equivalence given by Eqs (17) or (18) is valid, depending on whether an M-type or a C-type profile is taken. From the observed values $c_1 = 0.69 \pm 0.07$ and $c_2 = 1.66 \pm 0.10$, the condition

$$c_1 = c_2 - 1$$

is satisfied within error. Thus the original assumption of linearity between D and L seems reasonable. Since confidence limits of the fault displacement distribution coefficient are lower than that of the fault lengths, the best estimate for c, the 'regional' coefficient, is given by

$$c_2 = c_1 + 1 \text{ or } c_2 = 1.69 \pm 0.07 \text{ to 68\% uncertainty.}$$

The factor of proportionality γ (Eq. (3)) can be determined

$$\gamma = \left[\frac{(c_2 - 1)A}{c_2 - BG(\theta)}\right]^{\frac{1}{(c_2-1)}} (M\text{-type})$$

or

$$\gamma = \left[\frac{(c_2 - 1)A}{BG(\theta)}\right]^{\frac{1}{(c_2-1)}} (C\text{-Type}).$$

Hence

$$\gamma = 0.023 \pm 0.010 \ (M\text{-type})$$

$$\gamma = 0.049 \pm 0.030 \ (C\text{-type})$$

using derived values of $c_2 = 1.69$, $A = 3.36 \times 10^{-3}\ \mathrm{m}^{-0.31}$ and $B = 0.0288\ \mathrm{m}^{-0.31}$. $G(\theta) = 0.646$ is calculated from the orientation distribution of the large-scale fault lengths and the strikes of the sampling traverses at Trysunda (070°) and Storön (010°). These two estimates provide bounds on the estimate of γ, since it is expected that the actual representative displacement profile for the area is some intermediate case of an M- and a C-type profile.

The distribution of fault displacements sampled in a two-dimensional seismic section is expected to be similar to the one-dimensional fault displacement distributions observed in the field (Eq. (15), or alternatively the one-dimensional term of Eq. (10)), modified by the orientation factor $G(\theta)$, and subject to the constraints of seismic resolution.

SEISMIC MODELLING

Synthetic seismograms were generated for reflector models incorporating the statistics of the field data using fourth-order acoustic finite difference code, in order to investigate the resolution of the seismic method in sampling fault populations, and the predicted perturbation to seismic reflections caused by these faults.

The seismic scale

The scale of features in the crust contributing to observable seismic reflections is defined using *Fresnel zones* and the *Raleigh criterion*, corresponding to resolution in the *horizontal* and *vertical* directions, respectively.

A seismic reflection is a sum of contributions of energy from a finite volume in the Earth's crust. The Fresnel zone corresponds to the 'illuminated' area on a geological reflector in the horizontal plane (Berkout, 1984). For a reflector at depth z, imaged by seismic energy of wavelength λ, the Fresnel zone has a diameter given by:

$$d_{cmp} = \sqrt{2z\lambda + \lambda^2/4}.$$

Thus, in unmigrated data and for the case $z \gg \lambda$, features on the reflector are subject to a spatial averaging over lateral distances of around $\sqrt{2z\lambda}$. The effect of a 'perfect' migration is to reduce the effective path length z of the seismic energy to zero, and the lateral resolution thus becomes $\lambda/2$. In practise, the resolution of the migrated image will be limited by the resolution and accuracy of the velocity model used in the migration. The *Rayleigh criterion* implies that features can be resolved if their vertical size is greater than one quarter of the seimic wavelength.

The vertical and horizontal resolution limits, at 10 km depth and for a dominant wavelength of ~400 m, are 100 m and 2800 m, respectively. A seismic reflection can be considered as an average response of a roughly cylindrical volume of the Earth with vertical and horizontal dimensions of 100 m and 2800 m, respectively (i.e. all 'roughness' on the reflector surface within the Fresnel zone is averaged). For a two-dimensional seismic profile, relief on the reflector is observed from trace to trace as the illuminated area moves along the reflector in the plane of the section and averages different portions of the sill surface.

Since features smaller than these limits still have some scattering effect, all features of size greater than the sampling distances of the seismic data were considered. A sampling interval of 4 ms gives a vertical sampling distance of the order of 10 m, whilst the trace spacing (i.e. horizontal sampling) in Fig. 2 is 25 m.

Generating faulted surfaces

A synthetic reflector was generated by perturbing a horizon with a synthetic population of faults, chosen to have the same cumulative fault population as derived from the field data (Eq. (15)). The observed spatial distribution of faults (Fig. 10) was predominantly random with weak clustering. Faults were therefore placed at random points along the horizon, with random sense of displacement (north side up/down).

The method is illustrated in Fig. 11. D_1 and D_2 are the minimum and maximum fault displacements of interest (in this case 10 m and 1000 m, respectively), F_1 and F_2 the corresponding cumulative frequencies. Each fault is assigned a displacement D_i given by the root of the equation $F(D_i) - \mathrm{RND}_i = 0$, where RND_i is a random number in the interval $F_2 < \mathrm{RND}_i < F_1$. The total number of faults generated along a horizon of length x is

$$N_G = (F_1 - F_2)x.$$

Table 1 shows the numbers of 10, 100 and 1000 m faults predicted for a horizon 75 km long. Fault counts are predicted for regional distribution coefficient values $c = 1.62$, 1.69 and 1.76. Uncertainty in c of ± 0.07 gives variations in the number of faults of displacement 10 m or more over 75 km of ± 7, or $\pm 17\%$.

Figure 12(a) shows a synthetic reflector perturbed by $F(D)$ the fault displacement distribution expected to be sampled in a N–S-striking seismic profile in the Bothnian Bay. The cumulative frequency of the generated faults is

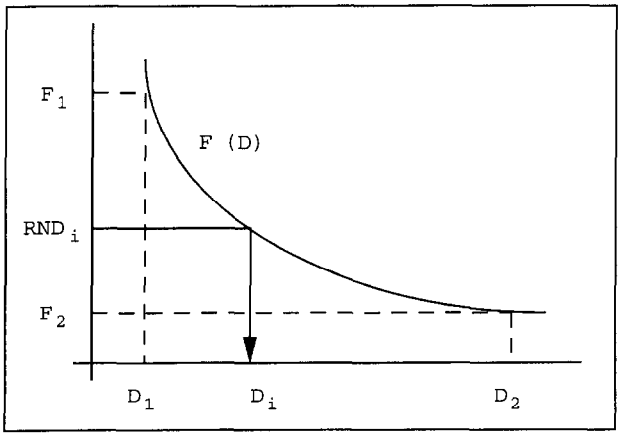

Fig. 11. Method of generating faults of random displacement, obeying a given cumulative frequency distribution. Each fault displacement D_i is a root to the equation $F(D' > D_i) - \mathrm{RND}_i = 0$ where RND_i is a random number between F_1 and F_2. D_1 and D_2 are minimum and maximum displacements of interest.

Table 1. Cumulative number of faults predicted along a 75-km long, N–S-striking horizon in the Bothnian Bay, for different values of regional fault distribution coefficient

	$N(D)$		
D (metres)	$c_2 = 1.62$	$c_2 = 1.69$	$c_2 = 1.76$
10	47.6	40.5	34.5
100	11.4	8.3	6.0
1000	2.7	1.7	1.0

consistent with the theoretical curve, and the faults have a spatial frequency along the reflector that is reasonably constant. Surface relief from faulting is very small, with only a few 100-m scale faults along the 75 km section. The relief is dominated by the largest faults; this is as one would expect for a power-law fault distribution with a two-dimensional coefficient of less than 2 (Jackson and Sanderson, 1992).

Finite difference modelling

'Exploding-reflector' synthetic seismograms were calculated using fourth-order acoustic code (Kelly *et al.*, 1976) available on the ProMax software of Advance Geophysical. Synthetic reflectors were discretised into a two-dimensional 25 m grid. In the 'exploding reflector method', a seismic wave is initiated at hypothetical sources along the reflector surfaces and propagated upwards at half the true Earth velocity. The seismogram measured at the top of the model (the 'Earth's surface') is equivalent to a plane wave reflection from the surface, or a CMP stack section.

A source wavelet with a dominant frequency of 15 Hz, and an Earth with a constant P-wave velocity of 6.0 km s^{-1} were used. The reflectors, placed at a depth of 6–7 km in the finite difference grid, were assigned a velocity 7.0 km s^{-1}. These parameters are consistent with the dominant frequency of the BABEL reflections, with upper crustal velocities in the Bothnian Bay, and with field velocity determinations of the dolerite. The synthetic seismograms were migrated, using a phase shift algorithm with a constant migration velocity of 6.0 km $^{-1}$.

RESULTS

A synthetic seismogram for the above section is shown in Fig. 12(b); 2 km at each end of the section, in which edge effects predominate, have been removed. The seismogram consists of a few continuous segments, bounded by large faults of displacement > 200 m. A few faults close to the limit of seismic resolution (~ 100 m) are visible within each segment.

Migrating the seismogram (Fig. 12c) increases the resolution of the seismogram. The sill appears as a

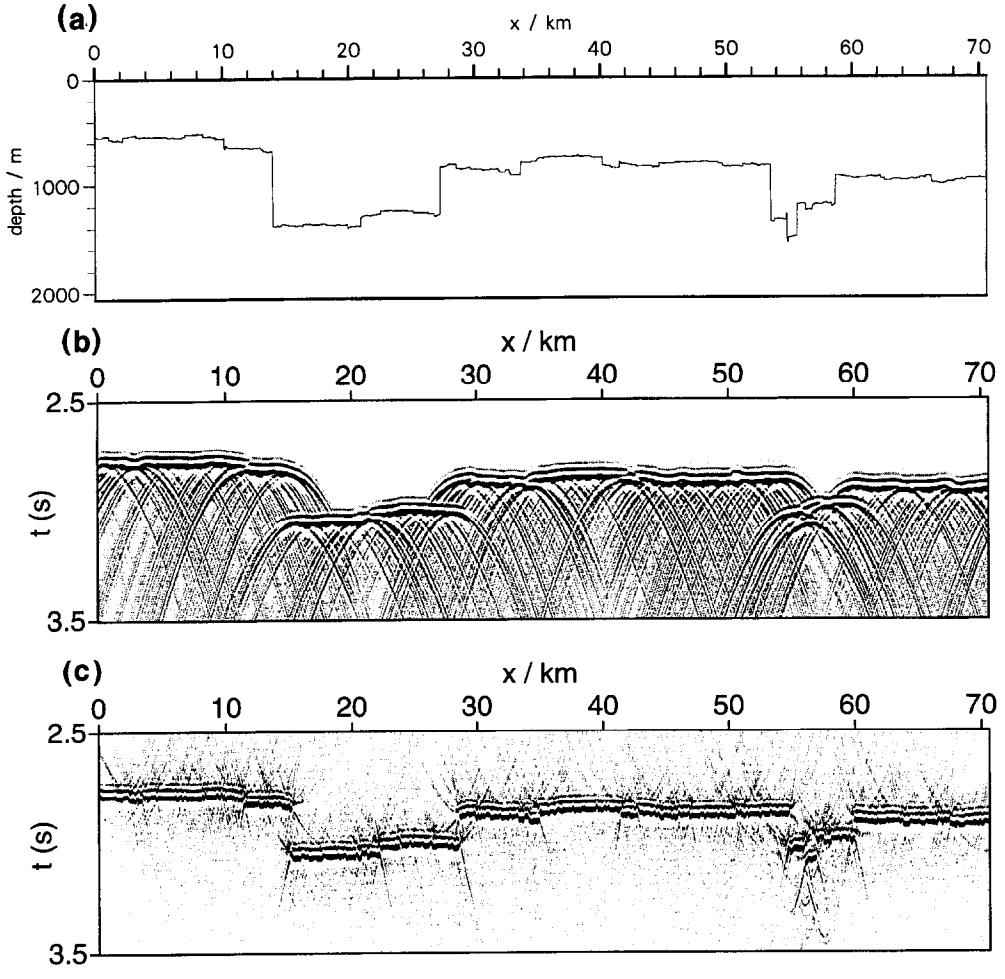

Fig. 12. (a)-N–S-striking random fractal surface, for a fault power-law distribution with coefficient 1.69. (b) The corresponding synthetic seismogram, bandpass-filtered 12–18 Hz. (c) The same seismogram migrated with a constant velocity of 6.0 km s^{-1}. The reflector is placed at 6–7 km depth in the finite difference model.

sequence of flat segments offset relative to each other by the large faults. Although more faults become visible within the segments, they are visible as small disruptions in the reflection horizon rather than as perceptible time shifts.

The field seismic data (Fig. 2) show a 5–30 km segmentation in reflections from the sills, and a 0.5–2 km-scale break-up in the individual reflection segments. The large-scale segmentation in the seismic section can be identified with either the primary segmentation of the sills evident on geological maps, or the segmentation arising from the large-scale faulting in Fig. 12(a). The predicted faulting in the sills leads to a weak small-scale loss in coherence (Fig. 12c). Neither this nor primary structural features in the sills are sufficient to account for the loss of coherence at the 0.5–2 km-scale evident in the BABEL data.

DISCUSSION AND CONCLUSIONS

The use of a single power-law in interpolating fault displacements and lengths over a wide range of scales is simplistic. Different processes will operate at the different scales and the microscopic properties of the rocks involved will differ to some extent from the macroscopic properties. Nevertheless, a power-law distribution is consistent with both fault lengths and displacements over more than 4 orders of magnitude and thus seems to be an adequate representation of these observed fault distributions. Furthermore, the good agreement in the respective exponents of the fault length and displacement distributions supports the underlying assumption of linearity between displacement and length. Although direct observations on fault length–displacement relationships are not possible in the field area, a method has been developed that allows an estimation of γ, the constant of proportionality, of 0.02–0.05. Uncertainty in this result is due to the unknown displacement profiles of faults in the area, which are likely to be highly variable.

The theoretical justification for a displacement/length linearity requires that the faults propagate in conditions of a uniform remote tectonic stress and a uniform lithology. Power-law distributions are only valid for a single fault population, rather than for several inherited ones. The bulk of the upper crust in the Svecofennian

province is generally of granitic, granodioritic and gneissic composition. The main faults in the area are considered to have been re-activated on several occasions in their tectonic history; in the field it was common to observe more than one set of slickenlines on a fault in the older rocks. However, the area has been relatively stable since the intrusion of the dolerite; faults of Jotnian age or younger, although poorly constrained in age, are assumed to have been subjected to similar stress fields. The obtained fault displacement and fault length distributions both infer a two-dimensional fault distribution coefficient of 1.69 ± 0.07 to 68% certainty and 1.69 ± 0.14 to 95% certainty. The observed fault spacing distribution implies that the faults at Trysunda and Storön are predominantly randomly spaced with a weak clustering. However, the complete function of fault clustering with respect to fault displacement remains poorly defined due to the limited numbers of faults mapped in 100% exposure. A synthetic fault population was randomly generated with the observed displacement distribution and a random spacing distribution. Although the spacing of faults in this population along a horizon is approximately constant, the reflector produced has similar features to that of a weakly clustered population; relief is small over most of the section and dominated in a few places by the largest faults of the population.

The synthetic seismic data show horizontal and vertical limits of resolution in the fault population that are consistent with the estimated Fresnel zone and Raleigh criterion, respectively. These resolution limits result in under-estimation of regional strain when interpreting faults from seismic data (Walsh *et al.*, 1991; Jackson and Sanderson, 1992). For instance, given a two-dimensional population exponent of 1.7, a maximum fault throw of 1000 m and a vertical resolution limit of 100 m, the strain calculated from the heave of approximately constant dip ($\sim 60°$) normal faults along a horizon is under-estimated by 40–50% (from Eq. (16), and Walsh *et al.*, 1991).

Qualitative comparison of the observed characteristics of the sills with their seismic reflections in BABEL line 1A/B would imply that the 5–30 km-scale segmentation in the reflections is partly a result of faulting, but is mainly an effect of primary segmentation of the sills. However, the observed fault displacements are at least an order of magnitude less than would be required to account for the smaller (< 5 km scale) segmentation of the seismic reflections in the BABEL data. The observed variability in the reflections over distances of less than 5 km is thus an imaging rather than a geological phenomenon. This loss of coherence may either be due to the processing of the seismic data, or because geological structures are being imaged through a complex medium with spatial variations in seismic velocity and density. Generally, the processing steps serve to increase, rather than decrease, the continuity of primary reflections; F/K filtering, CMP stacking (Gibson and Levander, 1988) and F/K migration are such examples. Thus the degradation in the coherence at the ~ 2 km-scale is attributed mainly to the scattering of seismic energy by impedance heterogeneity in the upper crust of the Baltic shield as it propagates through the overburden.

In summary, the observed fault populations in the Bothnian Sea imply that a substantial amount of regional strain is accommodated in faults that are smaller than the vertical seismic resolution of the sill reflections in the BABEL data. In areas where faults are more densely spaced, or more tightly clustered, the resolution of small faults would be further reduced by the limits in horizontal resolution of the seismic data, and also potentially by seismic scattering in the overburden. This emphasises the importance of integrating other methods into regional strain estimates that use seismic reflection data.

Acknowledgements—The authors would like to thank, for advice in aspects of the geology of the field area, Thomas Lundquist and Christopher Talbot—who is also thanked for his help in the field—and Carl-Erik Lund and others in the Institute of Earth Sciences & Department of Solid Earth Geophysics, Uppsala University for help in field logistics.

REFERENCES

Axberg, S. (1980) Seismic Stratigraphy and Bedrock Geology of the Bothnian Sea, North Baltic. *Stock. Contributions in Geology* **36**, 3.

BABEL Working Group (1993) Integrated seismic studies of the Baltic shield using data in the Gulf of Bothnia region. *Geophysical Journal International* **112**, 305–324.

Bergman, G. (1980) Quicksand structures in the Jotnian sandstone of central Sweden. *Geol. Fören. Stockh. Förh.* **102**, 111–116.

Berkout, A. J. (1984) *Seismic Resolution.* Geophys. Press, London.

Cowie, P. A. and Scholtz, C. H. (1992) Physical Explanation for the displacement–length relationship of faults using a post-yield fracture mechanics model. *Journal of Structural Geology* **14**, 1133–1148.

Gaal, G. and Gorbatchev, R. (1987) An Outline of the Precambrian Evolution of the Baltic Shield. *Precambrian Research* **35**, 15–52.

Gibson, B. S. and Levander, A. R. (1988) Modelling and processing of scattered waves in seismic reflection surveys. *Geophysics* **53**, 466–478.

Gillespie, P. A., Howard, C. B., Walsh, J. J. and Watterson, J. (1993) Measurement and characterisation of spatial distributions of fractures. *Tectonophysics* **226**, 113–141.

Gorbatchev, R., Lindh, A., Solyore, Z., Laitakari, I., Aro, K., Lobach-Zhuchenko, S. B., Markov, M. S., Ivliev, A. I. and Bryhni, I. (1987) Mafic dyke Swarms of the Baltic Shield. In: *Marie Dyke Swarm*, eds H. C. Halls and W. F. Fahrig, pp. 361–372. *Special Paper Geological Association Canada* **34**.

Jackson, P. and Sanderson, D. J. (1992) The scaling of Fault displacements from the Badajoz–Cordoba shear zone, South West Spain. *Tectonophysics* **210**, 179–190.

Kakimi, T. (1980) Magnitude–frequency relation for displacement of minor faults and its significance in crustal deformation. *Bulletin Geological Survey, Japan* **31**, 467–487.

Kelly, K. R., Ward, R. W., Trietel, S. and Alford, R. M. (1976) Synthetic Seismograms: a finite difference approach. *Geophysics* **41**, 2–27.

Larson, S. (1973) Igneous layering in the Ulvö dolerite, ngermanland, central Sweden. *Geol. Fören. Stockh. Förh.* **95**, 407–409.

Larson, S. and Magnusson, K. (1976) The Magnetic and chemical character of the Fe–Ti oxides in the Ulvö dolerite, central Sweden. *Sver. geol. Unders.* C **723**.

Larson, S. and Magnusson, K. (1979) A gravity investigation of the dolerite area on the coast of Angermanland, Sweden. *Geol. Fören. Stockh. Förh.* **101**, 1–16.

Laslett, G. M. (1982) Censoring and edge efffects in areal and line transect sampling of rock joint traces. *Mathematical Geology* **14**, 125–140.

Lundquist, T. (1973) Potash Feldspar megacrysts of a granite at Skaggsudde, central Sweden. *Sver. geol. Unders.* C **687**.

Lundquist, T. and Samuelsson, L. (1973) The differentiation of a dolerite at Nordingrå, central Sweden. *Sver. geol. Unders.* C **692**.

Magnusson, K. (1983). A petrophysical and Paleomagnetic study of the Nordingrå region in Eastern Sweden. *Sver. geol. Under* C **801**.

Marrett, R. and Allmendinger, R. W. (1991) Estimates of strain due to brittle faulting: sampling of fault populations. *Journal of Structural Geology* **13**, 735–738.

Marrett, R. and Allmendinger, R. W. (1992) Amount of extension on 'small' faults: an example from the Viking Graben. *Geology* **20**, 47–50.

Muraoka, H. and Kamata, H. (1983) Displacement distribution along minor fault traces. *Journal of Structural Geology* **5**, 483–495.

Peacock, D. C. P. (1991) Displacements and segment linkage in strike-slip fault zones. *Journal of Structural Geology* **13**, 1025–1035.

Peacock, D. C. P. and Sanderson, D. J. (1991) Displacements, segment linkage and relay ramps in normal fault zones. *Journal of Structural Geology* **13**, 721–733.

Pickering, G., Bull, J. M., Sanderson, D. J. and Harrison, P. V. (1994) Fractal fault displacements: A case study from the Moray Firth, Scotland. In: *Fractals and Dynamic Systems in Geosciences*, ed. J. H. Kruhl, pp. 105–119. Springer-Verlag, Frankfurt.

Pollard, D. D., Muller, O. H. and Dockstader, D. R. (1975) The form and growth of fingered sheet intrusions. *Bulletin Geological Society, America* **86**, 351–363.

Pollard, D. D. and Segall, P. (1987) Theoretical displacements and stresses near fractures in rock: with application to faults, joints, veins, dikes and solution surfaces. In: *Fracture Mechanics of Rock*, ed. B. K. Atkinson, pp. 277–349. Academic Press, New York.

Scholz, C. H. and Cowie, P. A. (1990) Determination of total strain from faulting using slip measurements. *Nature* **346**, 837–839.

Scholz, C. H., Dawers, N. H., Yu, J.-Z., Anders, M. H. and Cowie, P. A. (1993) Fault growth and fault scaling laws: Preliminary results. *Journal of Geophysical Research* **98**, 21951–21961.

Walsh, J. J. and Watterson, J. (1987) Distributions of cumulative displacement and seismic slip on a single normal fault system. *Journal of Structural Geology* **9**, 1039–1046.

Walsh, J. J., Watterson, J. and Yielding, G. (1991) The importance of small-scale faulting in regional extension. *Nature* **351**, 391–393.

Watterson, J., Walsh, J. J., Gillespie, G. A. and Easton, S. (1995) Scaling systematics of fault sizes on a large-scale range fault map. *Journal of Structural Geology* **18**, 199–214.

Welin, E. and Blomquist, G. (1964) Age measurements on radioactive minerals from Sweden. *Geol. Fören. Stockh. Förh.* **86**, 33–50.

Welin, E. and Lundquist, T. (1970) New Rb–Sr age data for the sub-Jotnian volcanics (Dala pophyries) in the Los-Hamra region, central Sweden. *Geol. Fören. Stockh. Förh.* **92**, 35–39.

Welin, E. and Lundquist, T. (1975) K–Ar ages of Jotnian dolerites in Västernorrlands County, central Sweden. *Geol. Fören. Stockh. Förh.* **97**, 83–88.

Winterhalter, B. (1972) On the geology of the Bothnian Sea, an epeiric sea that has under-gone Pleistocene Glaciation. *Geological Survey of Finland Bulletin* **258**.

Winterhalter, B., Floden, T., Ignatius, H., Axberg, S. and Niemisto, L. (1980) Geology of the Baltic Sea. In: *The Baltic Sea*, ed. A. Voipio, pp. 1–21. Elsevier Oceanography series, Helsinki.